Topics in Catalysis (2018) 61:902–914
https://doi.org/10.1007/s11244-018-0955-9

ORIGINAL PAPER

Synthesis of Chiral Dendrimer-Encapsulated Nanoparticle (DEN) Catalysts

Zhihuan Weng[1,2] · **Francisco Zaera**[1]

Published online: 11 May 2018

Abstract
Several synthetic strategies were developed for the preparation of chiral dendrimer-encapsulated Pt nanoparticle (Pt DEN) catalysts. In one approach, regular OH-terminated polyamidoamine (PAMAM) dendrimers were first derivatized with cinchonidine using "click" chemistry and sebacic acid as a linker. As many as half of the 64 terminal OH groups in a 4th generation PAMAM dendrimer could be modified this way, and the overall cinchonidine content could be tuned by controlling the CD:PAMAM ratio during synthesis. Platinum nanoparticles were then added to these cinchonidine-modified dendrimers. In an alternative route, regular Pt DENs were made first using PAMAM, and the resulting material was then derivatized with cinchonidine. The two synthetic routes proved successful, but led to materials with different spectroscopic and catalytic properties, presumably because the metal nanoparticles in the first case are made near the cinchonidine functionality, in the outside of the dendrimer structure rather than in its inside, as believed to be the case with the second procedure. A potential complication related to the poisoning of the Pt nanoparticle surface during synthesis was also identified in the second protocol. The catalytic performance of these catalysts for the hydrogenation of α-ketoesters proved to be poor in all cases, presumably because of a number of problems associated with mass transport limitations inside the dendrimer structures and restricted flexibility of the outer chiral branches, which may not be able to interact with the catalytic surfaces. Nevertheless, interesting synthetic lessons were derived from our work with potential value for other applications.

Keywords Platinum · Cinchonidine · Enantioselectivity · Infrared absorption spectroscopy · NMR · Asymmetric hydrogenation · Coupling reactions

1 Introduction

One of the central challenges in modern heterogeneous catalysis is the control of selectivity, as a way to minimize the consumption of reactants, the need for separation steps to purify the products, and the disposal of potentially toxic byproducts [1–3]. Perhaps the ultimate test regarding selectivity is the ability to synthesize catalysts capable of performing catalytic processes enantioselectively [4–7]. Much of the chemistry used to make enantiopure chiral compounds, especially in the pharmaceutical industry, uses homogeneous catalysts, but it would be highly desirable to substitute those with appropriate heterogeneous counterparts, which would be simpler to handle [8]. Unfortunately, efforts to develop heterogeneous chiral catalysts have to date resulted in limited success. Perhaps the best-known example is the so-called Orito reaction [9], in which a platinum-based hydrogenation catalyst is chirally modified by adding a small amount cinchona alkaloid to the feedstock solution [10–12]. This approach has been shown to lead to enantiomeric excesses in the chiral products quite close to 100%, but only for a very limited to reactants (typically α-ketoesters) [13]. It is also not an entirely heterogeneous process, as the cinchona alkaloid modifier is provided in solution and needs to be separated from the products afterwards.

Inspired by the Orito reaction, we have been exploring different ways to add the chiral modifiers directly to

Contribution for the Special Issue honoring Prof. Gabor A. Somorjai.

✉ Francisco Zaera
zaera@ucr.edu

[1] Department of Chemistry and UCR Center for Catalysis, University of California, Riverside, CA 92521, USA

[2] Present Address: Department of Polymer Science & Engineering, Dalian University of Technology, Dalian, People's Republic of China

solid catalysts. For instance, we have developed ways to tether cinchonidine to silica porous supports using well-established "click" chemistry [14–16] and have tested the resulting materials for the promotion of the enantioselective addition of aromatic thiols to unsaturated ketones [17, 18]; some examples are already available in the literature on the promotion of coupling reactions this way [19, 20]. We have also incorporated our click-chemistry synthetic methodology into a procedure for the modification of platinum/silica catalysts for the promotion of the Orito reaction [21], an approach also tried by others [22–25] (our unique contribution there has been to envision a way to tether the cinchona modifiers selectively next to the Pt nanoparticles dispersed on the silica support). In an attempt to design these bifunctional catalysts in a more integral manner, we have also tested the use of self-assembly to add the cinchona alkaloid directly to the surface of the metal [26]. The idea of using self-assembly to modify catalytic surfaces in order to improve selectivity has been advanced recently for other systems [27], and there is an interesting report where an asymmetric catalyst was prepared by encapsulating metallic nanoclusters in chiral self-assembled monolayers immobilized on a mesoporous SiO_2 support [28].

In this article, we report results from our study on a different approach, where enantioselectivity in the behavior of dendrimer-encapsulated metal nanoparticles (DENs) is attempted by modifying the dendrimer organic structure, adding a chiral agent to it. Dendrimers have proven to be quite useful in catalysis by themselves [29], thanks to the fact that they combine the molecularity that provides such control of selectivity in homogeneous catalysis with the ease of manipulation that comes from their high molecular weight [30]. There has also been some work specifically directed at making chiral dendrimers [31, 32]. Chirality can be added directly into the monomeric units used to build up the dendrimers, but that has turned out to be inefficient; a more viable approach has been to add chiral moieties to the end of achiral dendritic cores. To avoid problems with interference of the chiral functionality with the dendritic fragments at different generations, alkyl chains or rigid hydrocarbon backbones have been incorporated as spacers [33]. This is the approach chosen for our work: by using "click" chemistry, we have added cinchonidine (CD) moieties, which are chiral, to the end of OH-terminated polyamidoamine (PAMAM) dendrimers by using sebacic acid (SA) as the linker. We have further expanded our work to make dendrimer-encapsulated Pt nanoparticles (DENs) with the intention of testing those for enantioselective hydrogenation catalysis. The synthesis and evaluation of DENs have been successfully pioneered by the Crooks group [34], and have been tried for catalytic applications by many other research groups [35–42]. In the next sections, we describe the synthetic strategies that we have used for the preparation of our CD-based Pt-DEN catalysts and the results obtained from their characterization.

2 Synthesis of Cinchonidine-Terminated Dendrimers

The first step in our strategy was to develop an efficient way to prepare cinchonidine-terminated dendrimers. As mentioned in the introduction, we have done this by adding the cinchonidine (CD) molecules to our 4th-generation hydroxyl-terminated (G_4-OH_{64}) PAMAM dendrimers via "click" chemistry. Several linkers were tested for this purpose. To take advantage of our expertise on the use of click chemistry to tether cinchona alkaloids and other catalysts to silica solid surfaces [17, 18, 43], we first tried the use of propyltriethoxysilane-based linkers. We wanted to take advantage of our knowledge on how to control the tethering point of cinchonidine to the dendrimer: at the alcohol moiety (using a mercapto linkers), or at the peripheral vinyl group (that can react with an isocyanato functionality). The click chemistry was also tested in both possible sequences, namely, by attaching the CD to one end of the linker first and then the combined CD-linker unit to the PAMAM dendrimer, or by switching the order of these steps and binding the linker to the PAMAM first and adding the CD afterward. Unfortunately, the attachment of either the linker alone or the CD-linker unit to the dendrimer required in these protocols did not work: mass spectrometry data (taken using matrix-assisted laser desorption/ionization—MALDI) did not show any signal for masses above that of the pure PAMAM, and no evidence for the presence of the linker or the CD moiety could be extracted from any of the ^{1}H of ^{29}Si NMR spectra taken.

Based on the initial negative results with silane-based linkers, we moved on to using sebacic acid (SA, HOOC–C_8H_{16}–COOH), to form a carbamate link with the OH group in CD at one end and a second connection at the terminal hydroxyl ending of the PAMAM at the other. The CD–SA complex was made first, according to the following synthesis:

1. Cinchonidine (CD, 0.735 g, 2.5 mmol), sebacic acid (SA, 1.01 g, 5.0 mmol) and 4-(dimethylamino)pyridine (DMAP, 0.061 g, 0.5 mmol) were added to a 100 mL two-neck flask;
2. The flask was evacuated and filled with N_2;
3. 30 mL of tetrahydrofuran (THF), dried by using a molecular sieve, were added while maintaining the flask in an ice bath and under continuous stirring;
4. *N,N*-dicyclohexylcarbodiimide (DCC, 1.236 g, 6.0 mmol), dissolved in 20 mL of THF, was added dropwise;

5. After 30 min, the temperature of the mixture was increased to 300 K, and the reaction was continued under N_2 for 24 h;
6. The mixture was filtered to remove the solid, and the solvent of the filtrate was removed under reduced pressure; another 50 mL $CHCl_3$ were then added to dissolve all of the residual compounds;
7. The solution was sequentially washed with deionized water (3 × 50 mL), dried with Na_2SO_4 overnight, concentrated under reduced pressure, and further purified by using a silica column with ethyl acetate/THF/methanol as the diluent. The final product was a white solid.

This intermediate CD–SA product was characterized by infrared absorption spectroscopy, ^{1}H and ^{13}C NMR, and electrospray ionization (ESI) mass spectrometry; the data from the first two studies are provided in Figs. 1 and 2, with the corresponding peak assignments listed in Tables 1 and 2, respectively, and the mass spectrum is shown in Fig. 3.

This CD–SA sub-unit was then tethered to the PAMAM dendrimer according to the following procedure:

1. A solution of PAMAM-$(OH)_{64}$ (4th generation, 10 wt% in methanol, 0.86 g, [OH] = 0.386 mmol) was placed in a 100 mL two-neck flask, and the methanol was removed under reduced pressure;
2. CD–SA (0.2219 g, 0.463 mmol; 1.2 times the amount of OH groups in the PAMAM) was added;
3. The flask was evacuated and filled with N_2;

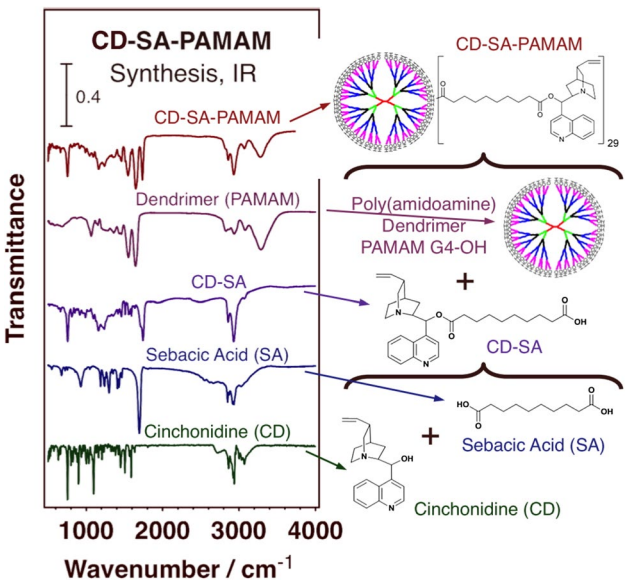

Fig. 1 Transmission infrared (IR) absorption spectra for the samples obtained at each step of the synthesis of our cinchonidine-modified polyamidoamine dendrimers (CD–SA–PAMAM). A scheme of the synthetic steps used is provided on the right

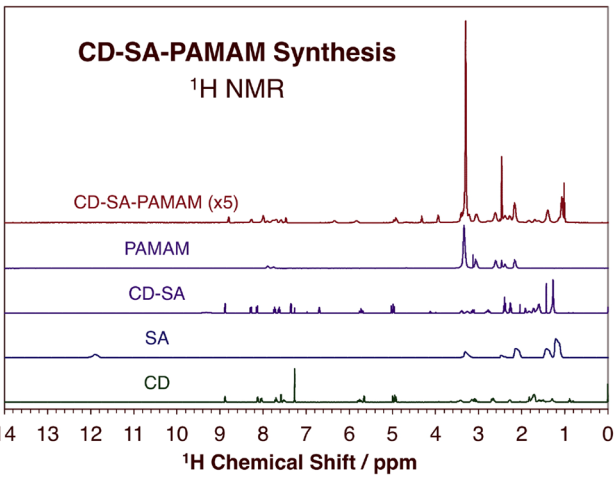

Fig. 2 ^{1}H NMR data for the same samples as in Fig. 1

4. Anhydrous dimethyl sulfoxide (DMSO, 10 mL) was added as a solvent;
5. DMAP (56.5 mg, 1.2 × 0.386 mmol) and *N*-(3-dimethylaminopropyl)-*N*′-ethylcarbodiimide (EDC, 0.1480 g, 2 × 0.386 mmol) were added into the solution;
6. The reaction was conducted at 313 K for 24 h while stirring under N_2;
7. The solvent was partially evaporated via evacuation;
8. The reaction solution was dialyzed for 2 days in ethanol using a cellulose dialysis tubing having a molecular weight cut off of 2000, changing the solvent every 8 h to remove impurities and residual reagents;
9. The residual solution in the dialysis tubing was collected, washing the tubing with ethanol several times. All these solutions were combined;
10. The ethanol solvent was removed under reduced pressure, and the product was dried by lyophilization.

The new products were characterized again by infrared absorption and ^{1}H NMR spectroscopies; the data are shown in Figs. 1 and 2, and the peak assignments provided in Tables 1 and 2. These data attest to our success in producing clean CD–SA–PAMAM samples with the procedure described above. To notice in particular are the disappearance of the C=O stretching mode in the IR data (at 1705 cm^{-1}, lost upon esterification) and the SA–CD peaks assigned to the –OH group in the ^{1}H NMR spectra (peak a at 9.32 ppm) after the last linking step. Also, the broad IR feature at 3299 cm^{-1}, attributed to the stretching vibration of the peripheral –OH groups in PAMAM, can still be seen in the trace of the final product, but at a reduced intensity. This suggests that the derivatization of the terminal hydroxyl groups in the PAMAM is only partial, a subject that we discuss in more detail next.

Table 1 Vibrational mode assignment for the infrared absorption spectra shown in Fig. 1

Assignment[a]	CD	SA	CD–SA	PAMAM	CD–SA–PAMAM
	CD modes [44]				
$\omega_{oop}(C–H)_Q$	757(vs)		757(vs)		756(vs)
$\omega_{oop}(C–H)_{QB}$, $\delta_{oop,Q}$	803(s)		817(s)		817(w)
$\omega_{oop}(C–H)_Q$	883(s)		885(s)		885(vw)
$\omega_{oop}(C–H)_{QB}$	1001(m)		991(w)		988(w)
$\delta_{ip,ring,Q}$, $\delta_{ip}(C–H)_Q$	1507(w)		1511(w)		1510(vw)
$\delta_{ip,ring,Q}$, $\delta_{ip}(C–H)_Q$	1590(m)		1597(m)		1593(vw)
$\nu(C–H)_{vinyl}$	2865(w)		2857(w)		2858(w)
$\nu(C–H)_{QB}$	3071(w)		3075(w)		3072(w)
	SA modes				
$\gamma(C–H)_{CH_2}$		1186(m)	1160(m)		1163(m)
$\omega(C–H)_{CH_2}$		1239(m)	1234(m)		1241(m)
$\nu(C=O)_{ester}$			1745(m)		1736(m)
$\nu(C=O)_{acid}$		1698(vs)	1705(m)		
$\nu_s(C–H)_{CH_2}$		2924(m)	2932(m)		2930(m)
	PAMAM modes				
$\nu(C–N)$				1553(vs)	1553(vs)
$\nu(C=O)$				1645(vs)	1647(vs)
$\nu(O–H)$				3288(vs)	3299(vs)

All frequencies reported in wavenumbers (cm^{-1}). Intensities given in parenthesis: vw = very weak; w = weak; m = medium; s = strong; vs = very strong

[a]Vibrational modes: ω = wagging; δ = deformation; ν = stretching; γ = scissoring. Subindices: oop = out-of-plane; ip = in-plane; Q = quinoline ring in CD; QB = benzene moiety of quinoline ring in CD; vinyl = vinyl moiety in quinuclidine of CD

The molecular weight average and distribution of the synthesized CD–SA–PAMAM samples were estimated by using MALDI-MS. As can be seen in Fig. 4, a broad feature was seen in those spectra centered around 27,500 amu, with a total width of approximately 14,000 amu. By using 14,277 and 478 g/mol as the values for the molecular weights of PAMAM-OH and SA–CD, respectively, and by realizing that one water molecule is lost in each esterification reaction between a PAMAM terminal hydroxyl and a CD–SA carboxyl group, we were able to calculate the average number of cinchonidine attachments achieved in our synthesis per PAMAM molecule to be approximately 30 ± 10, close to half of the 64 –OH groups in the 4th-generation PAMAM used in this study. Such estimate is in qualitative agreement with the reduction in intensity of the O–H stretching-mode peak (~3290 cm^{-1}) seen in the IR spectra of PAMAM upon the addition of the cinchonidine (Fig. 1).

The total number of cinchonidine molecules tethered to the individual PAMAM dendrimer units can be controlled by adjusting the ratio of the CD–SA and PAMAM reactants used in the coupling step. The initial experiments were performed with a x = CD–SA:PAMAM ratio of 1.2 as indicated above. Lower ratios were explored as well, as a way to lower the CD content in the derivatized dendrimer below the ~50% saturation obtained initially. It was found that, indeed, the average number of CD molecules incorporated into the PAMAM changes in an approximately linear fashion with the amount of CD–SA added to the reaction mixture. This is illustrated by the data in Fig. 5, which shows IR spectra for three CD–SA–PAMAM samples, made with x = 0.25, 0.5, and 1.2 ratios. It can be seen there that the intensity of the peaks due to the CD–SA unit increase in relative intensity (compared to those due to PAMAM) with increasing value of x; notice in particular the growth of the features at 880 and 1740 cm^{-1}, associated with the out-of-plane quinoline-ring C–H deformation and ester C=O stretching vibrational modes of the tethered CD–SA moieties. Corroborating information was obtained by using ^1H NMR (data not shown). One important consequence of these changes in CD:PAMAM ratios is that they alter solubility: with small CD contents, the dendrimers are typically soluble in high polarity solvents such as water, DMSO, or methanol, but as the number of CD moieties per PAMAM unit is increased, that solubility decreases. For instance, the signal intensities of the peaks in UV–Visible absorption spectra associated with cinchonidine, at 204, 226, 232, 285, and 320 nm, are lower with the x = 0.5 sample than with the x = 0.25 (Fig. 6). Conversely, the solubility in lower-polarity solvents such as chloroform was found to improve with the number of CD substitutions.

Table 2 ^{1}H NMR peak assignment for the spectra shown in Fig. 2

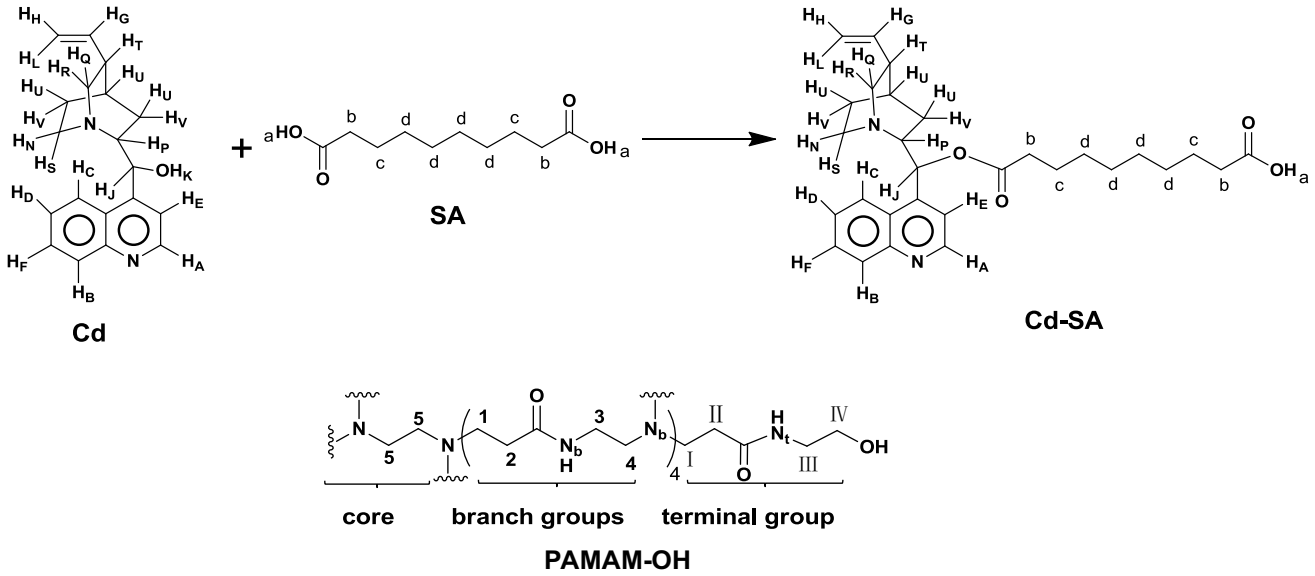

Chemical shift (ppm)	CD	SA	CD–SA	PAMAM	CD–SA–PAMAM
	CD peaks				
A	8.88		8.88		8.80
B	8.14		8.29		8.28
C	8.05		8.16		8.0
D	7.70		7.75		7.75
E	7.59		7.65		7.59
F	7.52		7.36		7.47
G	5.80		5.77		5.83
J	5.76		6.70		6.35
K	5.66		–		–
L	4.99		5.02		4.97
M	4.95		4.99		4.92
N	3.42		3.40		3.40
P	3.16		3.27		3.23
Q	3.09		3.13		3.22
R	2.70		2.81		Overlay
S	2.66		2.78		2.78
T	2.28		2.27		2.28
U	1.72–1.82		1.73–1.83		1.84
V	1.22–1.32		1.43		1.39
	SA peaks				
a		11.89	9.32		Disappear
b		2.15	2.40		Overlay
c		1.43	1.60		1.61
d		1.21	1.27		1.08
	PAMAM peaks				
5				4.68	4.69
3/III				3.07	3.07
1/I				2.61	2.61
4				2.39	2.39
2/II				2.17	2.17

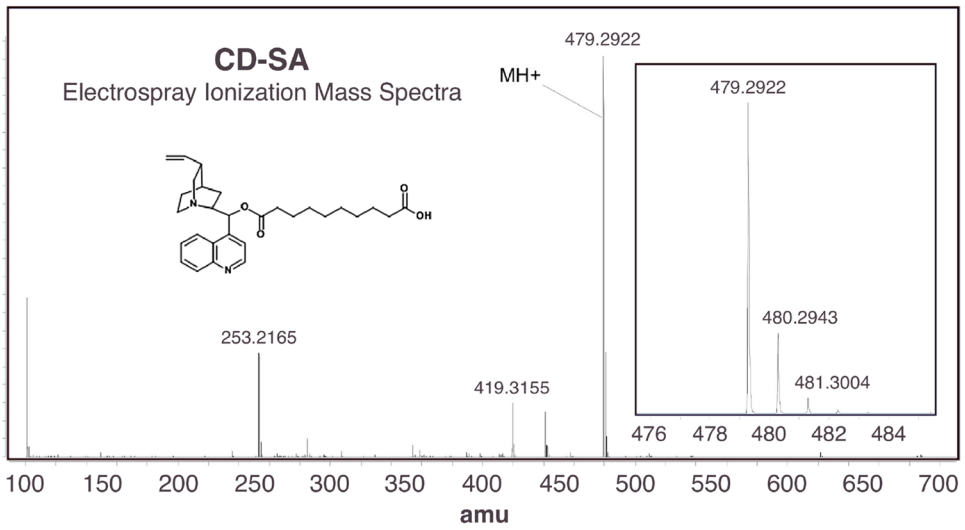

Fig. 3 Electrospray ionization (ESI) mass spectrum of the sebacic acid-derivatized cinchonidine (CD–SA)

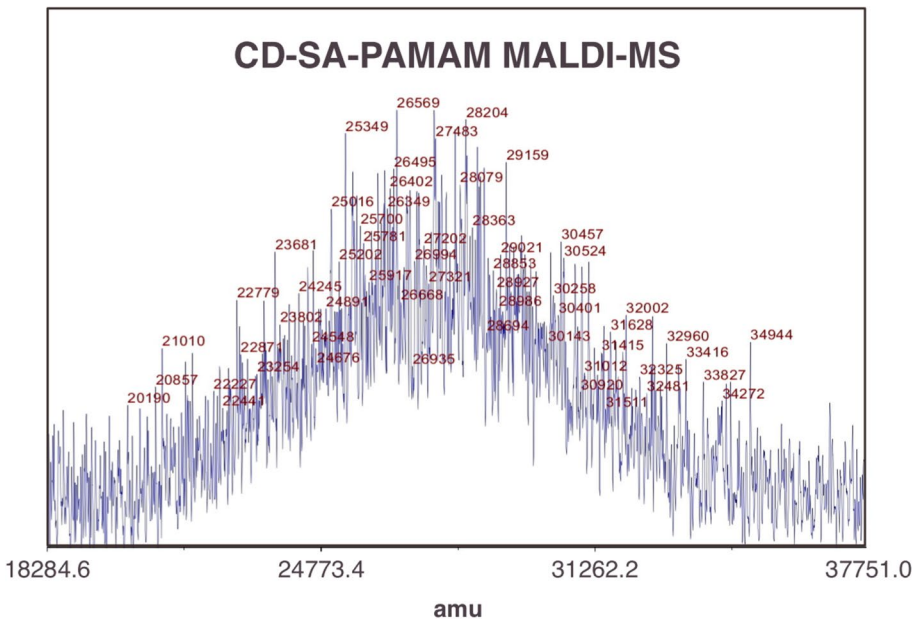

Fig. 4 Matrix-assisted laser desorption/ionization (MALDI) mass spectrum of the cinchonidine derivatized dendrimers (CD–SA–PAMAM) synthesized in this research

3 Synthesis of Cinchonidine-Terminated-Dendrimer Encapsulated Pt-Nanoparticles

Metal nanoparticles can be grown inside dendrimer structures via titration of the basic groups in the latter using a metal anion, $PtCl_4^{2-}$ in the case of platinum, followed by a reduction step, in a well-established protocol developed by the Crooks group [35]. In our case, the metal can be added either before or after the chiral modification of the dendrimer with cinchonidine. We found that both approaches present unique challenges, and that they lead to final materials with different catalytic properties. For the case where the platinum nanoparticles (Pt-NPs) were grown on the chirally-modified CD–SA–PAMAM, the synthetic steps were as follows:

1. 60 mg of CD–SA–PAMAM (2.18×10^{-6} mol) were dissolved in 21.8 mL DMSO;
2. The flask was evacuated and filled with N_2;
3. 36.2 mg of K_2PtCl_4 (8.72×10^{-5} mol, 40 equiv. to CD–SA–PAMAM, in 3 mL DMSO) were added dropwise into the solution;
4. The flask was sealed, and the reaction was conducted under dark for 10 days while continuously stirring (at the end of this step, the solution was yellow);
5. 33 mg of $NaBH_4$ (10 equivalents to K_2PtCl_4, in 10 mL DMSO) were added (the color of mixture changed to brown/black);

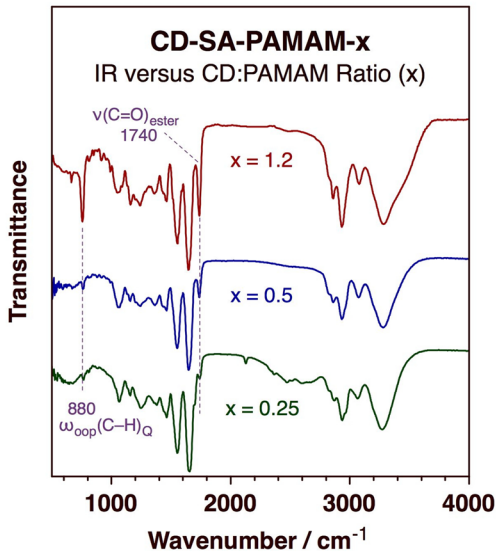

Fig. 5 Transmission IR absorption spectra for three CD–SA–PAMAM samples prepared using three different ratios of CD–SA versus PAMAM (x = 0.25, 0.5, and 1.2) in their synthesis. It is seen that the average number of CD substitutions per PAMAM unit increases approximately linearly with that ratio, as indicated by the growth of the peaks at 880 and 1740 cm^{-1}

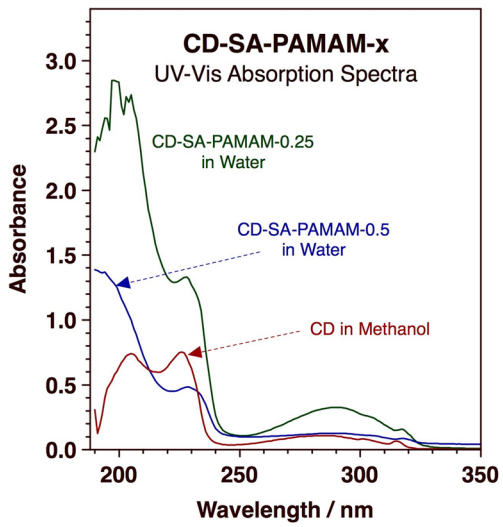

Fig. 6 UV–Vis absorption spectra for saturation solutions of CD–SA–PAMAM in water, used to evaluate their solubility. Data are provided for two samples, prepared with CD–SA:PAMAM (x) ratios of 0.25 and 0.5. A reference spectrum is also provided for pure cinchonidine (CD). The solubility decreases with increasing CD content in the PAMAM, as indicated by the lower signal obtained for the x = 0.5 sample (compared to the x = 0.25)

6. The reaction was continued for another 3 h
7. The solution was concentrated under vacuum, and purified by dialysis using DMSO and ethanol, with a cellulose dialysis tubing having a molecular weight cut off of 2000, changing the solvent every 8 h to remove impurities and residual reagents.

The incorporation of the Pt salt into the derivatized dendrimers was initially tested using the CD–SA–PAMAM-1.2 (the one prepared with a CD–SA:PAMAM ratio of x = 1.2) sample, and the expected chemistry was corroborated by UV–Vis absorption spectroscopy and by the observation that the product precipitated from solution as a yellow solid. The formation of the Pt nanoparticles after the reduction step also became evident by the change in color of that solid, to brown/black, and by the visualization of Pt nanoparticles with an average diameter of about 1.3 nm (~ 75 ± 35 Pt atoms) in transmission electron microscopy (Fig. 10; Table 3). Additional confirmation came from infrared absorption spectroscopy data, on the basis that the relative intensities of the peaks at 1558 and 1645 cm^{-1}, due to the amide-II N–H bending/C–N stretching and amide-I C=O stretching vibrations of the dendrimer, change upon the formation of the Pt nanoparticles inside the PAMAM dendrimers, and that the amide-I peak blue-shifts by about 10 cm^{-1} [45]. The data in Fig. 7, which displays IR spectra for both a regular PAMAM and for CD–SA–PAMAM-0.25 before and after the addition of the Pt nanoparticles, shows the expected changes: the 1645/1558 peak intensity ratios go from 1.4 to 0.75 in the original PAMAM and from 1.3 to 0.94 with CD–SA–PAMAM upon Pt-NP addition.

Although the synthesis of these PtNP–[CD–SA–PAMAM] chirally-modified DENs appears to have been successful, some potential pitfalls were identified with the synthetic approach, as it was determined that the $PtCl_4^{2-}$ ions coordinate preferentially to the quinuclidine nitrogen atoms in CD rather than to the internal amido groups of the PAMAM, as desired. Indeed, independent experiments with CD–SA indicated that similar Pt nanoparticles can be made with the isolated cinchonidine units, with comparable kinetics. Moreover, the peak at 255 nm, attributable to the ligand-to-metal charge transfer from the tertiary amines of the dendrimer to bound Pt^{2+} [35], could not be detected in the UV–Vis spectra of the PtNP–[CD–SA–PAMAM] samples (Fig. 9). Spectral changes similar to those seen upon addition of the platinum salt to the CD–SA–PAMAM (a disappearance of the broad feature at 285 nm and the growth and sharpening of the peaks at 305 and 315 nm) could be induced by titrating the CD amine groups with HCl as well, as previously reported [46] (data not shown). In retrospect, the tendency for the platinum ions to coordinate to CD is not surprising, given that the amine nitrogen atom in CD exhibits a higher pKa than the nitrogen atoms in PAMAM. It was established that this problem could be minimized (but perhaps not completely eliminated) by using the CD–SA–PAMAM samples with the lower CD loads, as those are soluble in water and can therefore be treated with the platinum salt directly in

Table 3 Catalytic performance of various catalysts for the hydrogenation of ethyl pyruvate

Entry	Catalyst	$n_{Catalyst}$ (mmol)	$V_{Solvent}$ (mL)	Pt/CD molar ratio	$t_{Reaction}$ (h)	Conversion (%)	%ee (±0.8)[a]	$<d>_{PtNP} \pm$ stdev (nm)	<# Pt>
1	1 wt% Pt/SiO_2	0.005	5	3	2.5/4	90.2/98.2	73.4		
2	PtNP–PAMAM	0.01	10	3	36	97.3	19.5	1.4 ± 0.2	95 ± 41
3	PtNP–PAMAM	0.01	10	–	36	98.5	0.6		
4	PtNP–[CD–SA–PAMAM-1.2] in DMSO	0.0038	5		28	97.5	0.4	1.2 ± 0.2	60 ± 30
5	PtNP–[CD–SA–PAMAM-1.2] in ethanol/water	0.0038	5		48	20.3	0.8	1.5 ± 0.2	120 ± 60
6	PtNP–[CD–SA–PAMAM-0.25] in water	0.0038	5		10/24	73.1/76.4	0.3	1.3 ± 0.2	75 ± 35
7	CD–SA–[PtNP–PAMAM] prepared in DMSO	0.0038	5		3/24	1.3/8.6	0.7	1.7 ± 0.2	170 ± 60
8	CD–SA–[PtNP–PAMAM] prepared in DMSO	0.0038	5	3	24	3.9			
9	CD–SA–[PtNP–PAMAM] prepared with DCC	0.0038	5		24	31.7			
	Effect of solvent								
10	PtNP–PAMAM in acetic acid	0.005	5	3	24	97.4	20.9		
11	PtNP–PAMAM in acetic acid + ethanol	0.005	5	3	24	30.7	10.0		
12	PtNP–PAMAM in ethanol	0.005	5	3	24	63.3	3.9		
	Effect of CD:Pt ratio								
13	PtNP–PAMAM	0.005	5	7.5	24	68.7	10.5		
14	PtNP–PAMAM	0.005	5	1	24	3.4	12.1		
	Effect of H_2 pressure								
15	PtNP–PAMAM ($P(H_2) = 1$ atm)	0.005	10	3	12	47.0	29.9		
16	PtNP–PAMAM ($P(H_2) = 10$ atm)	0.005	10	3	4.5	63.4	21.0		
17	PtNP–PAMAM ($P(H_2) = 30$ atm)	0.005	10	3	4.5	43.1	5.2		

Substrate (EtPy)/Catalyst molar ratio = 250/1, Solvent: acetic acid (unless otherwise indicated), T = 293 K, $P(H_2) = 1$ atm (unless otherwise indicated)

[a]Enantioselectivity excess toward the production of R-ethyl lactate

an homogeneous mixture (K_2PtC_4 is not very soluble in the alcohols needed to dissolve the CD–SA–PAMAM-1.2 sample, so water–alcohol mixtures were used in that case).

In order to circumvent the problem of the preferential coordination of the Pt ions to the external CD sites in the CD–SA–PAMAM samples, an alternative route was explored where the cinchonidine was added to the dendrimers after the formation of the Pt nanoparticles instead, to make what we denote as CD–SA–[PtNP–PAMAM] samples. Regular PtNP–PAMAM was first prepared as follows:

1. PAMAM was dissolved in 18 MΩ cm Milli-Q water;
2. The flask was evacuated and filled with N_2;
3. 36.2 mg of K_2PtCl_4, as a 0.1 M aqueous solution (40 equivalents per PAMAM), were added dropwise;

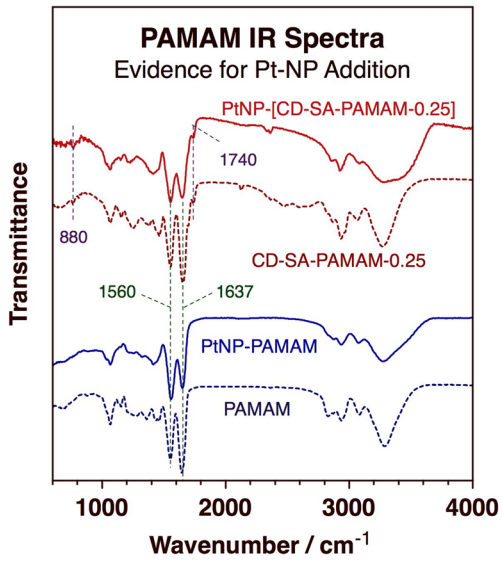

Fig. 7 Transmission IR absorption spectra for regular PAMAM and for our chirally-modified CD–SA–PAMAM-0.25 sample before and after the addition of the Pt nanoparticles, which was made evident by the change in relative intensities of the amide-II versus amide-I peaks, at 1560 and 1637 cm^{-1}, respectively. The presence of CD in the chirally-modified samples is also indicated by the peaks at 880 and 1740 cm^{-1}

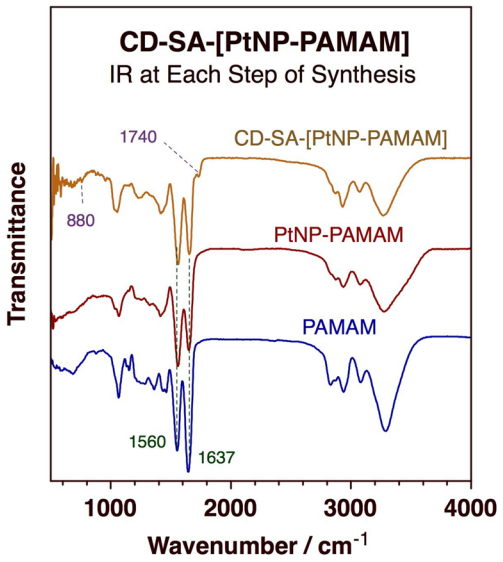

Fig. 8 Transmission IR absorption spectra at the different stages of the synthesis of the sample made by first preparing PtNP–PAMAM DENs, starting from a regular PAMAM, and then adding the cinchonidine chiral modifier. The success of the preparation procedure is indicated by both the changes in the relative intensity of the 1560 and 1637 cm^{-1} peaks upon the formation of the Pt nanoparticles and by the appearance of the new features at 880 and 1740 cm^{-1} indicative of the addition of the CD–SA moieties

4. The flask was sealed, and the reaction was conducted under dark while stirring for 10 days (the color of the solution changed gradually from pink to yellow, a progression that was followed by UV–Vis);
5. 33 mg of $NaBH_4$, as a 0.15 M fresh aqueous solution (10 equivalents to K_2PtCl_4), were added into the resulting solution (the color of the mixture changed to black);
6. The reaction was continued for 3 h;
7. The solution was concentrated under vacuum, and purified by dialysis using H_2O_2, with a cellulose dialysis tubing having a molecular weight cut off of 2000, changing the solvent every 8 h to remove impurities and residual reagents.

Once the PtNP–PAMAM were made, the cinchonidine was added as follows:

1. 20 mg of the PtNP–PAMAM catalyst ([OH] = 5.8×10^{-5} mol, 35.3 wt% of Pt) was placed in a two-neck flask;
2. CD–SA (6.9 mg, 0.25 × [OH]) and DMAP (1.77 mg, 1 equivalent to CD–SA) were added;
3. The flask was evacuated and filled with N_2;
4. Anhydrous DMSO (6 mL) was added as a solvent;
5. EDC (22.2 mg, 2 × [OH]) was added;
6. The reaction was conducted at room temperature while stirring for 24 h;
8. The solution was concentrated under vacuum, and purified by dialysis for 2 days using ethanol, with a cellulose dialysis tubing having a molecular weight cut off of 2000, changing the solvent every 8 h to remove impurities and residual reagents.
7. The residual solution in the dialysis tubing was collected, washing the tubing with ethanol several times, and all the solutions were collected together;
8. The ethanol solvent was removed under reduced pressure, and the product was dried by lyophilization.

The success of this synthetic protocol was checked by IR and UV–Vis absorption spectroscopies; the data are shown in Figs. 8 and 9, respectively. Two things are worth noticing in the IR absorption spectra reported in Fig. 8, which corroborate the success of the synthesis of the CD–SA–[PtNP–PAMAM] sample. First, the ratio of the amido-I (~ 1637 cm^{-1}) to amido-II (~ 1560 cm^{-1}) peak intensities changes upon the addition of the Pt nanoparticles, from 1.4 on the free PAMAM to 0.76 and 0.80 for PtNP–PAMAM and CD–SA–[PtNP–PAMAM], respectively. This is indicative of the formation of the Pt nanoparticles inside the PAMAM dendrimer. Second, new peaks are seen in the spectra for CD–SA–[PtNP–PAMAM] at 880 and 1740 cm^{-1}, corroborating the success of the CD addition step. The most significant observations deriving from the UV–Vis absorption spectra reported in Fig. 9 is the appearance of a new band at 255 nm in the traces for PtNP–PAMAM and CD–SA–[PtNP–PAMAM], an absorption associated with a

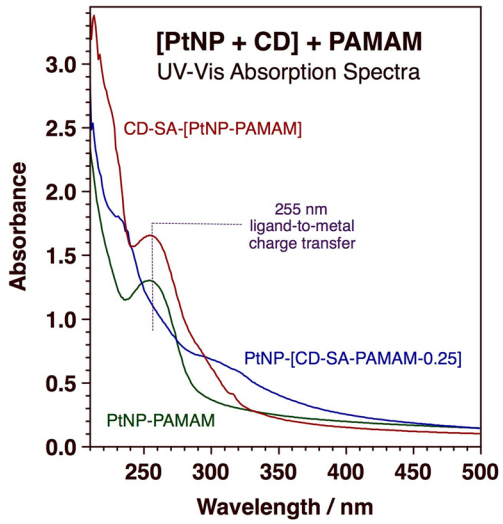

Fig. 9 Comparative UV–Vis absorption spectra for PtNP–[CD–SA–PAMAM-0.25] and CD–SA–[PtNP–PAMAM], that is, for cinchonidine-modified Pt DENs made by adding either the chiral modifier or the nanoparticles first, respectively. A reference spectrum for a regular PtNP–PAMAM DEN is provided as reference. To notice is the fact that a peak at 255 nm assigned to a ligand-to-metal charge transfer band is seen only in the samples where the cinchonidine is added last

ligand-to-metal charge transfer, and the increase in absorption at low energies because of the inter-band transition of the encapsulated zero-valent metal nanoparticles [35]. Notice that the spectrum for the PtNP–[CD–SA–PAMAM-0.25] sample, that is, for the sample where the Pt nanoparticles were added after the incorporation of cinchonidine into the dendrimer structure, shows more intensity at lower energies but no indication of complexation of the Pt(II) ions with the nitrogen atoms in the dendrimer (no 255 nm peak intensity), as we mentioned before. Finally, all methods yielded Pt nanoparticles of approximately the same size, with average diameters of about 1.5 nm (~ 120 ± 60 Pt atoms), as indicated by the TEM images in Fig. 10. The actual distributions of the NP diameters measured for each case are shown in each panel of Fig. 10, and the average values are listed in Table 3. Also reported there are the number of Pt atoms estimated from such diameters using the known values for the density (21.45 g/cc) and molecular weight (195.084 g/mol) of Pt.

4 Catalytic Performance

The new catalysts made in this project were tested for the catalytic promotion of the hydrogenation of ethyl pyruvate (EtPy) to ethyl lactate, with particular interest in the potential selectivity of our samples toward the production of the R enantiomer. A summary of the data obtained from these studies is provided in Table 3. The results are contrasted with measurements made with a standard 1 wt% Pt/SiO_2 catalyst, synthesized in house by wet impregnation of an Aerosil 200 commercial support (Degussa, 200 m^2/g) with $Pt(NH_3)_4Cl_2$.

The data in Table 3 clearly indicate that, unfortunately, none of the catalysts made here are better than a regular Pt/SiO_2 sample modified via the addition of cinchonidine from solution (Entry 1). That reference catalyst was capable of reaching almost full conversion within 4 h of reaction and of achieving an enantiomeric excess (ee) of close to 75% under the (non-optimized) conditions of our reaction. In contrast, the best CD-derivatized dendrimer-based catalyst, PtNP–[CD–SA–PAMAM-1.2] in DMSO (Entry 4), required approximately one full day to reach a similar conversion, and showed almost no %ee. Even the PtNP–PAMAM catalysts could not be chirally modified efficiently by adding CD to the reaction mixture in solution: the activity of that system was still significantly slower than that of the Pt/SiO_2 sample, and an enantioselectivity of only about 20% was possible (Entry 2). This would argue for limited access of the CD molecules to the center of the dendrimers, where the Pt nanoparticles reside. We have shown in the past that access to the Pt surface in Pt-DENs is certainly limited in the gas phase [47], but that it can be greatly enhanced in solution [48]. Moreover, a size-measuring study has reported a significant swelling of dendrimer structures in solution, and extensive access of water molecules to the inside of the dendrimers [49]. Yet, it would appear that the cinchonidine molecules cannot effectively reach the surface of the Pt nanoparticles in our catalysts. In addition, the CD molecules tethered to the outside layer of the dendrimers do not seem to provide an effective chiral environment for the platinum surface. It would appear that these CD terminations may limit access to the inside volume of the dendrimers, even if added in small amounts (as was done with the PtNP–[CD–SA–PAMAM-0.25] sample, Entry 6), and that they themselves cannot back-fold and reach the earlier-generation layers of the dendrimers, as it has been claimed happens with regular dendrimers [49].

A related issue hampering the performance of our chirally-modified dendrimer-based catalyst is their limited solubility. The effect of the solvent is illustrated by the different results reported in Entries 4 and 5 of Table 3, where the performance of the same PtNP–[CD–SA–PAMAM-1.2] catalyst is reported in two different solvents, DMSO and an ethanol/water mixture. Catalytic activity is clearly higher in the first solvent, where the solid shows higher solubility, even if this is not a good media for the reactant. By contrast, the more soluble PtNP–[CD–SA–PAMAM-0.25] catalyst performs better in water (Entry 6). Mass transport may therefore limit the performance of these catalysts. Entries 10–12 in Table 3, which report results from experiments with regular PtNP–PAMAM plus cinchonidine added to the reaction

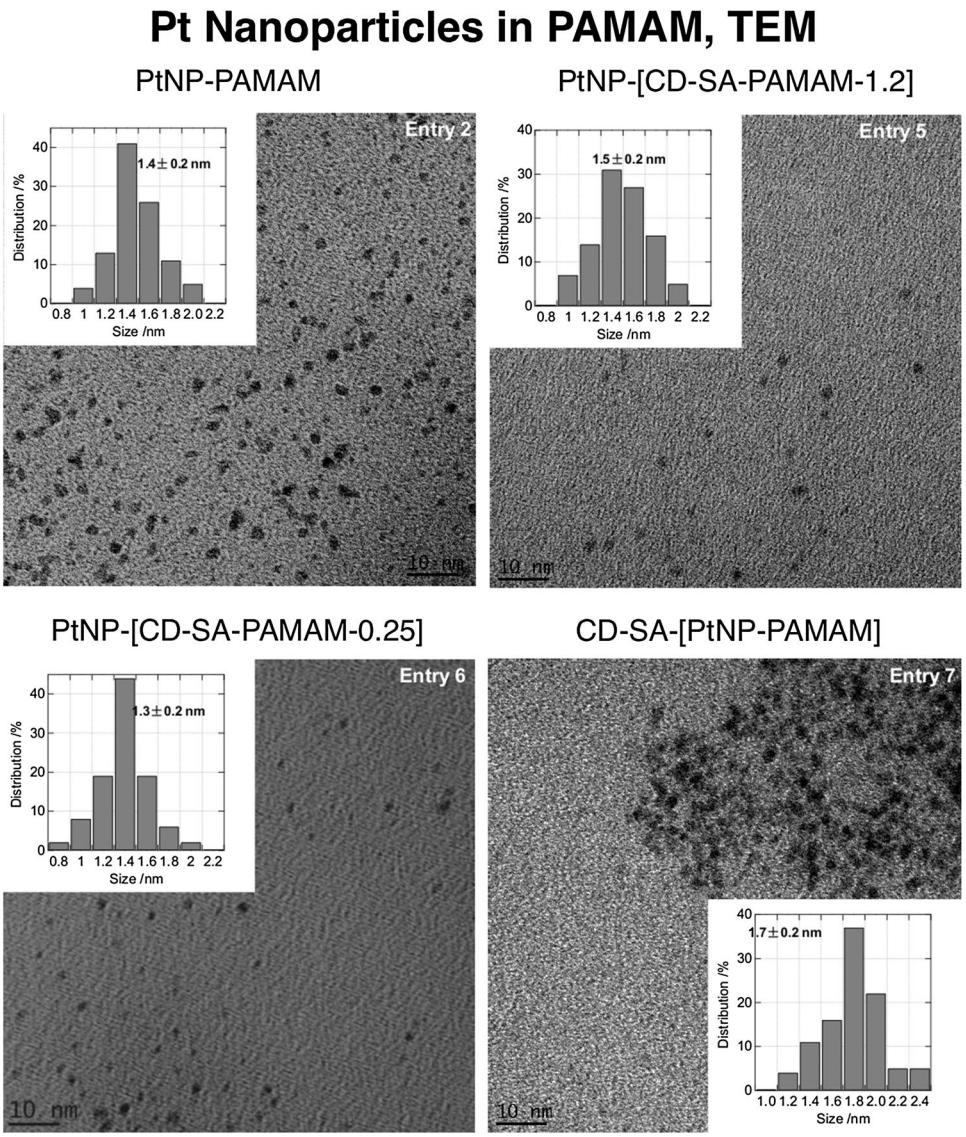

Fig. 10 Transmission electron microscopy (TEM) images of different CD-modified Pt-DENs. Also reported in the insets are the size distributions of the platinum nanoparticles measured from images like the ones shown (total nanoparticle count per distribution = 100). The entry numbers refer to Table 3

solution, also show that changing solvents affect the performance of these catalysts. The solvent is known to affect the efficiency of the Orito reaction even with regular platinum catalysts [50–53], but in this case there is an additional solubility factor to be considered. Unfortunately, only a handful of solvents could be tested, those where all the reactant, the chiral modifier, and the catalyst are soluble. Entries 13 and 14 attest to the fact that the relative amount of cinchonidine added to the reaction mixture is also an important parameter to consider [54, 55], but that the ratio chosen initially in our experiments was close to the optimum already.

The catalysts where cinchonidine was added to the dendrimer structure after forming the platinum nanoparticles inside, that is, where the chirality was attached directly to the Pt DENs, were the ones that showed the worst performance (Table 3, Entries 7–9). In that case, the length of the sebacic linker between the CD and the PAMAM, ~ 1.4 nm, needs to be added to the average distance between the surface of the Pt nanoparticles and the edge of the PAMAM dendrimers, which has been estimated to be ~ 0.7 ± 0.2 nm [34], to figure out how far the chiral modifier sits from the active catalytic centers: ~ 2.1 nm. However, the carbon chain of the sebacic acid linkers are quite flexible, so distance alone may not explain the poor catalytic performance of the CD–SA–[PtNP–PAMAM] catalysts. Certainly, adding cinchonidine to the reaction solution alone do not improve the catalytic performance of the CD–SA–[PtNP–PAMAM] sample (Entry 8 in Table 3). Instead, we suspect that the poor catalytic performance observed may be due to the fact that the surface of the platinum catalyst may become poisoned during the last synthetic steps, the one required to couple the CD–SA units to the PAMAM dendrimer. It may be that some of the reactants used in that synthesis poison the metal surface irreversibly. To test this possibility,

N,N′-dicyclohexylcarbodiimide (DCC) was used instead of *N*-(3-dimethylaminopropyl)-*N′*-ethylcarbodiimide (EDC) to attach the cinchonidine to the PtNP–PAMAM. Unfortunately, quite poor performance was obtained with that catalyst as well (Entry 9); the new carbodiimide appears to be as poisonous as the old, even though we initially argued that the added steric hindrance from the cyclohexyl rings in DCC could minimize the problem; inactivation of the platinum catalytic surface during the steps used for the addition of cinchonidine to the Pt DENs remains the most likely explanation for the particularly bad catalytic performance of the resulting CD–SA–[PtNP–PAMAM] samples.

A few additional tests were attempted in search of better results, with no success. For instance, it was seen that addition of the chirally-modified CD–SA–PAMAM dendrimer to the regular 1 wt% Pt/SiO_2 catalyst resulted in almost complete loss of catalytic activity. Larger Pt nanoparticles in the DENs, which were prepared by reducing the Pt^{2+}–PAMAM precursors with H_2 instead of $NaBH_4$ [56], also led to a reduction in activity and an almost complete loss of enantioselectivity. Larger (higher-generation) dendrimers were not considered here, as the resulting DENs have already proven to be less effective catalysts, presumably because of the increased distance between the metal surface and the edge of the PAMAM units [57]. Increasing the hydrogen pressure used during hydrogenation was found to indeed increase catalytic activity, but to also result in a loss of enantioselectivity (Table 3, Entries 15–17). The processing of larger α-ketoesters yielded less promising results: the hydrogenation of ethyl 2-oxo-4-phenylbutyrate with PtNP–PAMAM, with CD added to the solution, took 36 h for a 4.5 conversion, and resulted in negligible enantioselectivity (%ee = 1.7). Finally, the catalytic behavior of the cinchonidine functionality by itself in the CD-derivatized dendrimers was briefly probed. For this, we used a previously reported test reaction, namely, the addition p-tert-butylbenzenethiol to 2-cyclohexen-1-one [17, 18, 58, 59]. Full conversion was obtained within 24 h with both CD–SA–PAMAM and PtNP–[CD–SA–PAMAM], but with very poor enantioselectivity (%ee = 2.0 and 3.8, respectively). The reasons for this are at present unknown.

5 Conclusions

Successful protocols were developed for the preparation of chiral dendrimer-encapsulated metal nanoparticles (DENs). Two general approaches were tested, by first making cinchonidine-derivatized PAMAM dendrimers and then adding the metal nanoparticles, and by reversing that sequence, making regular DENs first and adding the cinchonidine modifier afterward. The two procedures were successful, but led to final samples with different catalytic properties. In the first case, the metal nanoparticles may be formed close to the outside of the dendrimer structure, not in the inside volume, because the complexation of the metal ion to the organic framework that is part of this synthesis is likely to occur at the cinchonidine endings newly attached to the dendrimers, not at the inside of the structure as expected. With the reverse (second) approach, the main problem is the potential poisoning of the metal nanoparticle surface with the reagents used to link cinchonidine to the dendrimer structure. Nevertheless, the success in obtaining the desired final structures was corroborated by a combination of spectroscopies (IR, UV–Vis, NMR, mass spectrometry) as well as by electron microscopy.

These samples proved to be poor catalysts for hydrogenation reactions, showing both low activities and limited if any enantioselectivities. These poor performances may be explained by a combination of factors, problems associated mainly with limited mass transport through the dendrimer structures and their low solubilities. Disappointing as these results are, they do not detract from the value of the lessons learned during the development of the synthetic protocols and the potential use of the chiral DENs for other applications such as chiral chromatography, biomolecular recognition, photo-switching, and as therapy or imaging agents for medical uses [60–64].

Acknowledgements Financial assistance for this project has been provided by grants from the U.S. National Science Foundation and the U. S. Department of Energy.

References

1. Zaera F (2009) Acc Chem Res 42:1152
2. Ye R, Hurlburt TJ, Sabyrov K, Alayoglu S, Somorjai GA (2016) Proc Natl Acad Sci USA 113:5159
3. Zaera F (2017) ACS Catal 7:4947
4. Hutchings GJ (2005) Annu Rev Mater Res 35:143
5. Baiker A (2015) Chem Soc Rev 44:7449
6. Gellman AJ, Tysoe WT, Zaera F (2015) Catal Lett 145:220
7. Zaera F (2017) Chem Soc Rev 46:7374
8. Blaser H-U (2010) Top Catal 53:997
9. Orito Y, Imai S, Niwa S (1980) J Chem Soc Jpn 670
10. Heitbaum M, Glorius F, Escher I (2006) Angew Chem Int Ed 45:4732
11. Mallat T, Orglmeister E, Baiker A (2007) Chem Rev 107:4863
12. Ma Z, Zaera F (2009) Chiral modification of catalytic surfaces. In: Ozkan US (ed) Design of heterogeneous catalysis: new approaches based on synthesis, characterization, and modelling. Wiley-VCH, Weinheim, pp 113–140
13. Bartók M (2006) Curr Org Chem 10:1533
14. Corma A, Garcia H (2006) Adv Synth Catal 348:1391
15. Copéret C, Basset J-M (2007) Adv Synth Catal 349:78
16. Pujari SP, Scheres L, Marcelis ATM, Zuilhof H (2014) Angew Chem Int Ed 53:2
17. Hong J, Lee I, Zaera F (2011) Top Catal 54:1340
18. Hong J, Zaera F (2012) J Am Chem Soc 134:13056

19. Corma A, Iborra S, Rodríguez I, Iglesias M, Sánchez F (2002) Catal Lett 82:237
20. Zhao W, Zhang Y, Qu C, Zhang L, Wang J, Cui Y (2014) Catal Lett 144:1681
21. Hong J, Lee I, Zaera F (2014) Catal Sci Technol 5:680
22. Blaser H-U, Jalett H-P, Müller M, Studer M (1997) Catal Today 37:441
23. Huang Y, Xu S, Lin VSY (2011) ChemCatChem 3:690
24. Azmat MU, Gue Y, Guo Y, Lu G, Wang Y (2012) J Porous Mater 19:605
25. Li X, Wu P (2014) Curr Org Chem 18:1242
26. Weng Z, Zaera F (2014) J Phys Chem C 118:3672
27. Kumar G, Lien C-H, Janik MJ, Medlin JW (2016) ACS Catal 6:5086
28. Gross E, Liu JH, Alayoglu S, Marcus MA, Fakra SC, Toste FD, Somorjai GA (2013) J Am Chem Soc 135:3881
29. Wang D, Astruc D (2013) Coord Chem Rev 257:2317
30. De Jesús E, Flores JC (2008) Ind Eng Chem Res 47:7968
31. Pittelkow M, Brock-Nannestad T, Moth-Poulsen K, Christensen JB (2008) Chem Commun 2358
32. Gade LH (2014) Molecular catalysts. Wiley-VCH Verlag GmbH & Co. KGaA, Weinheim, pp 407–422
33. Kassube JK, Gade LH (2006) Top Organomet Chem 20:61
34. Scott RWJ, Wilson OM, Crooks RM (2005) J Phys Chem B 109:692
35. Zhao M, Crooks RM (1999) Angew Chem Int Ed 38:364
36. Lang H, May RA, Iversen BL, Chandler BD (2003) J Am Chem Soc 125:14832
37. Huang W, Kuhn JN, Tsung C-K, Zhang Y, Habas SE, Yang P, Somorjai GA (2008) Nano Lett 8:2027
38. Zaera F (2013) ChemSusChem 6:1797
39. Lei W, Yu Z, Yi-Gang J (2013) Curr Org Chem 17:1288
40. Zaera F (2013) Chem Soc Rev 42:2746
41. Wang D, Deraedt C, Ruiz J, Astruc D (2015) Acc Chem Res 48:1871
42. Lim H, Ju Y, Kim J (2016) Anal Chem 88:4751
43. Hong J, Djernes KE, Lee I, Hooley RJ, Zaera F (2013) ACS Catal 3:2154
44. Chu W, LeBlanc RJ, Williams CT, Kubota J, Zaera F (2003) J Phys Chem B 107:14365
45. Liu D, Gao J, Murphy CJ, Williams CT (2004) J Phys Chem B 108:12911
46. Stimson MM, Reuter MA (1946) J Am Chem Soc 68:1192
47. Albiter MA, Zaera F (2010) Langmuir 26:16204
48. Albiter MA, Crooks RM, Zaera F (2010) J Phys Chem Lett 1:38
49. Maiti PK, Çağın T, Lin S-T, Goddard WA (2005) Macromolecules 38:979
50. Wehrli JT, Baiker A, Monti DM, Blaser HU, Jalett HP (1989) J Mol Catal 57:245
51. Meheux PA, Ibbotson A, Wells PB (1991) J Catal 128:387
52. Gamez A, Köhler J, Bradley J (1998) Catal Lett 55:73
53. Ma Z, Zaera F (2005) J Phys Chem B 109:406
54. LeBlond C, Wang J, Andrews AT, Sun Y-K (2000) Top Catal 13:169
55. Kubota J, Zaera F (2001) J Am Chem Soc 123:11115
56. Deutsch DS, Lafaye G, Liu D, Chandler B, Williams CT, Amiridis MD (2004) Catal Lett 97:139
57. Niu Y, Yeung LK, Crooks RM (2001) J Am Chem Soc 123:6840
58. Hiemstra H, Wynberg H (1981) J Am Chem Soc 103:417
59. Tian S-K, Chen Y, Hang J, Tang L, McDaid P, Deng L (2004) Acc Chem Res 37:621
60. Vögtle F, Gestermann S, Hesse R, Schwierz H, Windisch B (2000) Prog Polym Sci 25:987
61. Tekade RK, Kumar PV, Jain NK (2009) Chem Rev 109:49
62. Astruc D, Boisselier E, Ornelas C (2010) Chem Rev 110:1857
63. Mintzer MA, Grinstaff MW (2011) Chem Soc Rev 40:173
64. Kannan RM, Nance E, Kannan S, Tomalia DA (2014) J Intern Med 276:579